NEUROSCIENCE

Molecular basis of junctional current rectification at an electrical synapse

Yuan Shui, Ping Liu*, Haiying Zhan†, Bojun Chen, Zhao-Wen Wang‡

Rectifying electrical synapses (RESs) exist across animal species, but their rectification mechanism is largely unknown. We investigated why RESs between AVA premotor interneurons and A-type cholinergic motoneurons (A-MNs) in *Caenorhabditis elegans* escape circuit conduct junctional currents (I_j) only in the antidromic direction. These RESs consist of UNC-7 innexin in AVA and UNC-9 innexin in A-MNs. UNC-7 has multiple isoforms differing in the length and sequence of the amino terminus. In a heterologous expression system, only one UNC-7 isoform, UNC-7b, can form heterotypic gap junctions (GJs) with UNC-9 that strongly favor I_j in the UNC-9 to UNC-7 direction. Knockout of *unc-7b* alone almost eliminated the I_j, whereas AVA-specific expression of UNC-7b substantially rescued the coupling defect of *unc-7* mutant. Neutralizing charged residues in UNC-7b amino terminus abolished the rectification property of UNC-7b/UNC-9 GJs. Our results suggest that the rectification property results from electrostatic interactions between charged residues in UNC-7b amino terminus.

INTRODUCTION

Gap junctions (GJs) are intercellular channels that may permit the passage of ions and signaling molecules. GJs between neurons are generally referred to as electrical synapses (ESs) because they allow current flow between neurons. Although most ESs reported to date conduct currents bidirectionally, accumulating evidence indicates that many ESs are rectifying ESs that allow current flow predominantly or exclusively in one direction. Rectifying ESs were first found in crayfish (*1*) and subsequently found in additional teleost species (*2*, *3*), flies (*4*), lampreys (*5*), leeches (*6*, *7*), crabs (*8*), worms (*9*), and rats (*10*). Rectifying ESs may be much more prevalent than what has been appreciated because their existence can only be detected through electrophysiological recording (*10*, *11*). A variety of physiological functions have been attributed to rectifying ESs, including acting as coincidence detectors (*12*, *13*), promoting cooperativity of afferents to presynaptic neurons (*2*), and enhancing chemical synaptic transmission in mixed electrical-chemical synapses (*9*). Because rectifying ESs have the potential to affect neural circuit functions in complex ways, it is important to understand the molecular mechanisms of rectification.

GJs consist of connexins in vertebrates and innexins in invertebrates. Each GJ is a complex of two hemichannels, which are also known as connexons or innexons based on molecular compositions. Depending on whether the two hemichannels have identical molecular compositions, GJs are classified into homotypic and heterotypic GJs. Molecular compositions have been suggested for only a few rectifying ESs, including those between the giant fiber and motoneurons or interneurons in *Drosophila* (*4*), between auditory afferents and the Mauthner cells in goldfish (*2*), and between premotor interneurons and cholinergic motor neurons in *Caenorhabditis elegans* escape circuit (*9*). All these rectifying ESs appear to be heterotypic GJs of either two different GJ proteins (*2*, *9*) or two different isoforms of one GJ protein (*4*). However, it is unknown how junctional currents (I_j) are conducted preferably in one direction at rectifying ESs. One recent study showed that an intracellular scaffold protein localizes and functions exclusively on the postsynaptic side of ESs in the Mauthner cell system of zebrafish (*14*), but it is unknown whether the asymmetric scaffold localization plays a role in rectification. Another study (*15*) examined the effects of swapping the N termini (before the first transmembrane domain or TM1) between two different isoforms of the Shaking B innexin, Shaking B neural +16 (ShakBN16), and Shaking B Lethal (ShakBL), on GJ function using the *Xenopus* oocyte heterologous expression system. ShakBN16 and ShakBL are the putative pre- and postsynaptic GJ proteins, respectively, of the rectifying ESs in the fly giant fiber system (*4*). Substitution of the N terminus of ShakBL by that of ShakBN16 made the chimeric protein (SBL-NTN16) functions like ShakBN16 in heterotypic GJs with ShakBL. However, substitution of the N terminus of ShakBK16 by that of ShakBL did not make the chimeric protein to function like ShakBL in heterotypic GJs with ShakBN16. Furthermore, homotypic GJs of SBL-NTN16 resembled those of ShakBL instead of ShakBN16 in transjunctional voltage (V_j) dependence and I_j deactivation properties (*15*). It is difficult to tell from these results whether the N terminus plays a role in rectification. This difficulty is compounded by the fact that amino acid sequence differences between ShakBL and ShakBN16 are not restricted to the N terminus but extend all the way to TM2.

The GJs between a pair of premotor interneurons known as AVA and A-type cholinergic motor neurons (A-MNs) in *C. elegans* escape circuit present a unique opportunity for uncovering the molecular mechanism of electrical rectification for a combination of reasons. First, they conduct I_j almost exclusively in one direction (from A-MNs to AVA) (*9*). Second, their functional properties may be analyzed in vivo using dual-neuron voltage- and current-clamp techniques (*9*). Third, their molecular compositions on the pre- and postsynaptic sides may be genetically manipulated in a cell-specific manner. Previous studies have established that these GJs consist of UNC-7 innexin in AVA and UNC-9 innexin in A-MNs (*9*, *16*). However, UNC-7 has 10 different isoforms from alternative splicing.

Department of Neuroscience, University of Connecticut School of Medicine, Farmington, CT 06030, USA.
*Present address: Department of Pathophysiology, School of Basic Medicine and Tongji Medical College, Huazhong University of Science and Technology, Wuhan, China.
†Present address: Roswell Park Comprehensive Cancer Center, Department of Pathology, Elm and Carlton Street, Buffalo, NY 14263, USA.
‡Corresponding author. Email: zwwang@uchc.edu

It is unknown which UNC-7 isoform is important to the electrical coupling and why this coupling is strongly rectified. Here, we addressed these two questions through analyzing biophysical properties of homotypic and heterotypic GJs formed by UNC-9 and UNC-7 in *Xenopus* oocytes and analyzing the effects of isoform-specific or cell-targeted knockout, knockdown, and mutant rescue of *unc-7* on the function of the rectifying ESs in vivo. Our results led to the identification of a specific UNC-7 isoform, UNC-7b, as a key component of the rectifying ESs in the worm's escape circuit, and the proposition of a model in which a ball-and-receptor mechanism involving UNC-7b N terminus confers the rectification. This study shows a correlation of rectifying properties between GJs in vivo and in a heterologous expression system and presenting a molecular model for the rectification mechanism. Because major structural and functional properties are conserved between innexin- and connexin-based GJs (*17*, *18*), this study may provide insights into molecular mechanisms of GJ rectification in general.

RESULTS

Homotypic GJs formed by UNC-7 and UNC-9 differ in biophysical properties

To understand the molecular mechanism of I_j rectification between AVA and A-MNs, we began by analyzing biophysical properties of homotypic GJs formed by UNC-7 and UNC-9 in *Xenopus* oocytes. While UNC-9 has only one functional isoform (another isoform listed at the Wormbase website is unlikely to form GJs because it lacks the N terminus, TM1, and part of the first extracellular loop), UNC-7 has 10 isoforms (www.wormbase.org). The different UNC-7 isoforms may be divided into six groups based on their differences in the N terminus: UNC-7a/j, UNC-7b, UNC-7c, UNC-7d/e, UNC-7f/g, and UNC-7h/i (Fig. 1, A to C). The isoforms that are grouped together differ in only two consecutive amino acid residues, valine (V) and glutamine (Q), in the intracellular loop, which are present in the a, b, c, d, f, and h isoforms but not in the remaining isoforms. The N terminus before TM1 varies greatly in length among the UNC-7 variants, ranging from 24 amino acids in UNC-7c to 168 amino acids in UNC-7d/e (Fig. 1, B and C). UNC-7c resembles UNC-9 in the N terminus length (Fig. 1D).

We analyzed homotypic GJs formed by UNC-9 and six different UNC-7 isoforms (a, b, c, e, f, and h) representing the six groups. In each pair of oocytes expressing an identical innexin, a series of membrane voltage (V_m) steps were applied to one oocyte (oocyte #1) from a holding voltage of −30 mV, while the other oocyte (oocyte #2) was held constant at −30 mV to record I_j (Fig. 2A). V_j is defined as "V_m of oocyte #2 − V_m of oocyte #1". The relationship between steady-state junctional conductance (G_j) and V_j was fitted to a Boltzmann function (see Materials and Methods) to quantify V_0 (the V_j at which G_j is half maximal), G_{jmin} (the minimum G_j), and A (a cooperativity constant). Two different connexin 38 (Cx38) antisense oligonucleotides were always coinjected with *unc-7* and *unc-9* complementary RNAs (cRNAs) to eliminate potential complications by endogenous I_j (details in Materials and Methods). At least one pair of control oocytes, which had been injected with only the two oligonucleotides, was analyzed electrophysiologically on every day of recordings. Endogenous I_j were never detected from them, as exemplified by the recording of one such control experiment (fig. S1).

All the innexins were able to form homotypic GJs in *Xenopus* oocytes. These GJs displayed bidirectionally symmetric I_j (Fig. 2B) and bell-shaped G_j-V_j relationships (Fig. 2C) in response to the positive and negative V_j steps. However, they often differed in the apparent V_j dependence (the slope of the G_j-V_j curve) (Fig. 2C) and the V_0, G_{jmin}, and A parameters (Fig. 2D and table S1). They also differed in the I_j deactivation rate, as quantified from fitting the I_j traces at −110 and +110 mV V_j to two exponentials (Fig. 2E and table S2). On the basis of the apparent V_j dependence and G_{jmin} (Fig. 2C), the GJs may be grossly divided into two groups. Group 1 includes UNC-7c and UNC-9 while group 2 includes the remaining UNC-7 isoforms. Group 1 displayed much weaker V_j dependence and much larger G_{jmin} than group 2, as indicated by the quantitative comparisons (Fig. 2D). Because N terminus is shorter in group 1 than in group 2, these observations suggest that a longer N terminus may confer a higher degree of V_j dependence and a smaller G_{jmin}. However, it is not a simple linear relationship between N terminus length and V_j dependence. For example, UNC-7a was less V_j-dependent than both UNC-7e and UNC-7h but its N terminus is intermediate in length. Together, our observations suggest that V_j dependence depends on both the length and amino acid sequence of the N terminus.

Heterotypic UNC-7b/UNC-9 GJ is a strong rectifier

We next paired oocytes expressing UNC-9 with those expressing the different UNC-7 isoforms and recorded I_j from both oocytes. These heterotypic UNC-7/UNC-9 GJs often displayed bidirectionally asymmetric I_j in response to the positive and negative V_j steps, with I_j traces from one oocyte mirroring those from the other of the pair (Fig. 3A).

For simplicity, we focus on I_j recorded from the UNC-7 oocyte and the derived G_j-V_j relationship. The heterotypic GJs may be divided into two major groups according to whether the ascending and descending portions of the G_j-V_j curve are grossly symmetric. Group 1, including UNC-7f/UNC-9 and UNC-7h/UNC-9 GJs, showed a symmetric G_j-V_j relationship whereas group 2, including the remaining heterotypic GJs, showed an asymmetric G_j-V_j relationship (Fig. 3B). Group 2 may be further divided into two subgroups according to the position of the V_j corresponding to the apparent G_{jmax}. It was shifted to the left (negative V_j range) with UNC-7b/UNC-9 but to the right (positive V_j range) with UNC-7e/UNC-9, UNC-7c/UNC-9, and UNC-7a/UNC-9 (Fig. 3B). The differences between the G_j-V_j relationships of the different GJs can be better appreciated from quantitative comparisons of the V_0, G_{jmin}, and A parameters from the Boltzmann fit (Fig. 3C and table S3). The heterotypic GJs also differed in activation and deactivation rates, as quantified by fitting the I_j traces at −110 and +110 mV of V_j to exponentials (fig. S2A and table S4). Because molecular differences among these GJs are limited to variations in the UNC-7 N terminus, these results indicate that the N terminus of UNC-7 plays an important role in determining V_j dependence and other biophysical properties of the heterotypic GJs. Notably, UNC-7b/UNC-9 is the only one with the apparent G_{jmax} at a negative V_j. Given that $V_j = V_m$ of UNC-7 oocyte − V_m of UNC-9 oocyte as we defined, the results suggest that UNC-7b/UNC-9 GJs are more active than any of the other heterotypic GJs at the negative V_j range (when the UNC-9 oocyte is more depolarized than the UNC-7 oocyte).

UNC-7b/UNC-9 GJs differed from the other heterotypic GJs more notably in the peak I_j, which were measured within an identical time window for both the positive and negative V_j steps (fig. S2B). While the others allowed bidirectional peak I_j, UNC-7b/UNC-9 heterotypic GJs conducted peak I_j almost exclusively in the

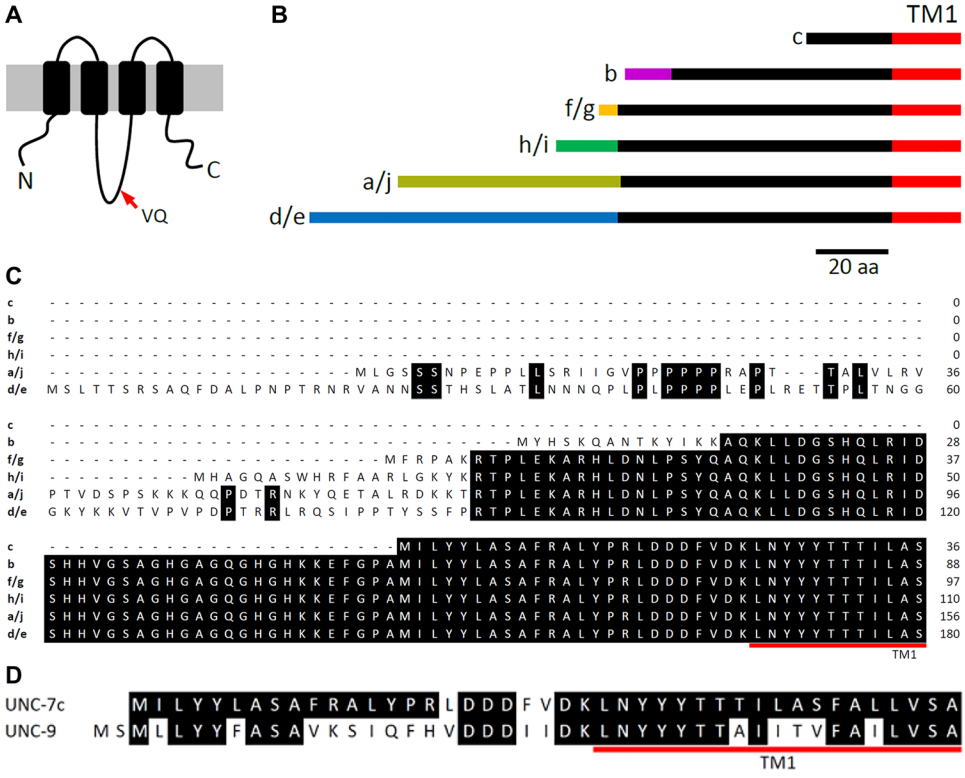

Fig. 1. UNC-7 isoforms differ mainly in the length and amino acid sequence of the N terminus. (**A**) Diagram showing the membrane topology of UNC-7 and the location of the variable valine and glutamine residues in the intracellular loop. (**B**) Diagram showing differences of UNC-7 N termini. Lines of an identical color represent identical amino acid sequences. aa, amino acid. (**C**) Alignment of the N termini of different UNC-7 isoforms. (**D**) Alignment of the N termini of UNC-7c and UNC-9.

direction from the UNC-9 oocyte to the UNC-7 oocyte (Fig. 3A), as indicated by the detection of large I_j from the UNC-7 oocyte at negative V_j but from the UNC-9 oocyte at positive V_j. The difference in peak I_j rectification between UNC-7b/UNC-9 and the other heterotypic GJs can be more easily appreciated by comparing normalized I_j-V_j relationships (Fig. 3D) and the ratio of peak I_j at −110 and +110 mV (Fig. 3E). Because the peak I_j of UNC-7a/UNC-9 GJs were symmetric between the positive and negative V_j ranges, their I_j-V_j curve was used as a reference for statistical comparisons, which show that the peak I_j of UNC-7b/UNC-9 and UNC-7h/UNC-9 GJs are significantly rectified with the degree of rectification being far greater in the former than the latter (Fig. 3D). Calculation of the peak I_j ratio (−110/110 mV) for recordings from the UNC-7 side shows that the ratio was significantly higher in UNC-7b/UNC-9 and UNC-7h/UNC-9 GJs than in UNC-7a/UNC-9 GJs (Fig. 3E). In rare instances, the peak I_j of UNC-7h/UNC-9 and UNC-7f/UNC-9 heterotypic GJs also showed strong rectification, as indicated by the scatter plot in Fig. 3E and sample I_j traces in fig. S3. UNC-7f and UNC-7h are more similar to UNC-7b in the length of the N terminus than the other UNC-7 isoforms (Fig. 1, B and C). Because UNC-7b/UNC-9 GJs showed strong rectification in both the steady state and peak I_j and favored I_j flow in the same direction as that in vivo (from A-MNs expressing UNC-9 to AVA expressing UNC-7) (*9*), our results suggest that UNC-7b is likely a key component of the UNC-7/UNC-9 GJs between AVA and A-MNs.

UNC-7b is important to AVA/A-MN coupling

To confirm the putative role of UNC-7b in AVA/A-MN coupling, we first expressed green fluorescent protein (GFP) reporter under the control of *unc-7b* promoter (P*unc-7b*) to infer the expression pattern of UNC-7b. A homologous recombination approach was used in this experiment to include all potential P*unc-7b* sequence. Specifically, we constructed a plasmid that included a short fragment of DNA sequence before the initiation site of *unc-7b* and a portion of the *unc-7b* first exon fused in-frame to GFP. This plasmid was coinjected with a fosmid containing 32.7 kb genomic DNA sequence upstream of the *unc-7b* initiation site into an existing strain with AVA labeled by mStrawberry (*9*). Homologous recombination between the plasmid and fosmid in vivo would result in a *Punc-7b::GFP* transcriptional fusion (Fig. 4A, left). In transgenic worms, GFP expression was observed in many neurons in the head including the two AVA interneurons (Fig. 4A, right), suggesting that UNC-7b is expressed in AVA.

We next analyzed the effect of *unc-7b* knockout on AVA/A-MN coupling in partially immobilized worms. The *unc-7b* was knocked out in wild-type worms by mutating lysine 14 (K14) codon to a premature stop using the CRISPR-Cas9 approach. Dual-neuron voltage clamp experiments were performed to record I_j between AVA and VA5, which was selected as a representative of A-MNs because it can be more easily identified based on anatomy than other A-MNs (Fig. 4B, left). Identification of AVA was based on AVA-specific GFP expression (Fig. 4B, right). In wild-type worms, I_j recorded from AVA were predominantly in the inward direction, whereas those from VA5 were predominantly in the outward direction in response to V_j steps from −80 to +80 mV (Fig. 4C). I_j between AVA and VA5 were undetectable in *unc-7(e5)* (Fig. 4D) and reduced by >70% in the *unc-7b* knockout strain compared with wild type

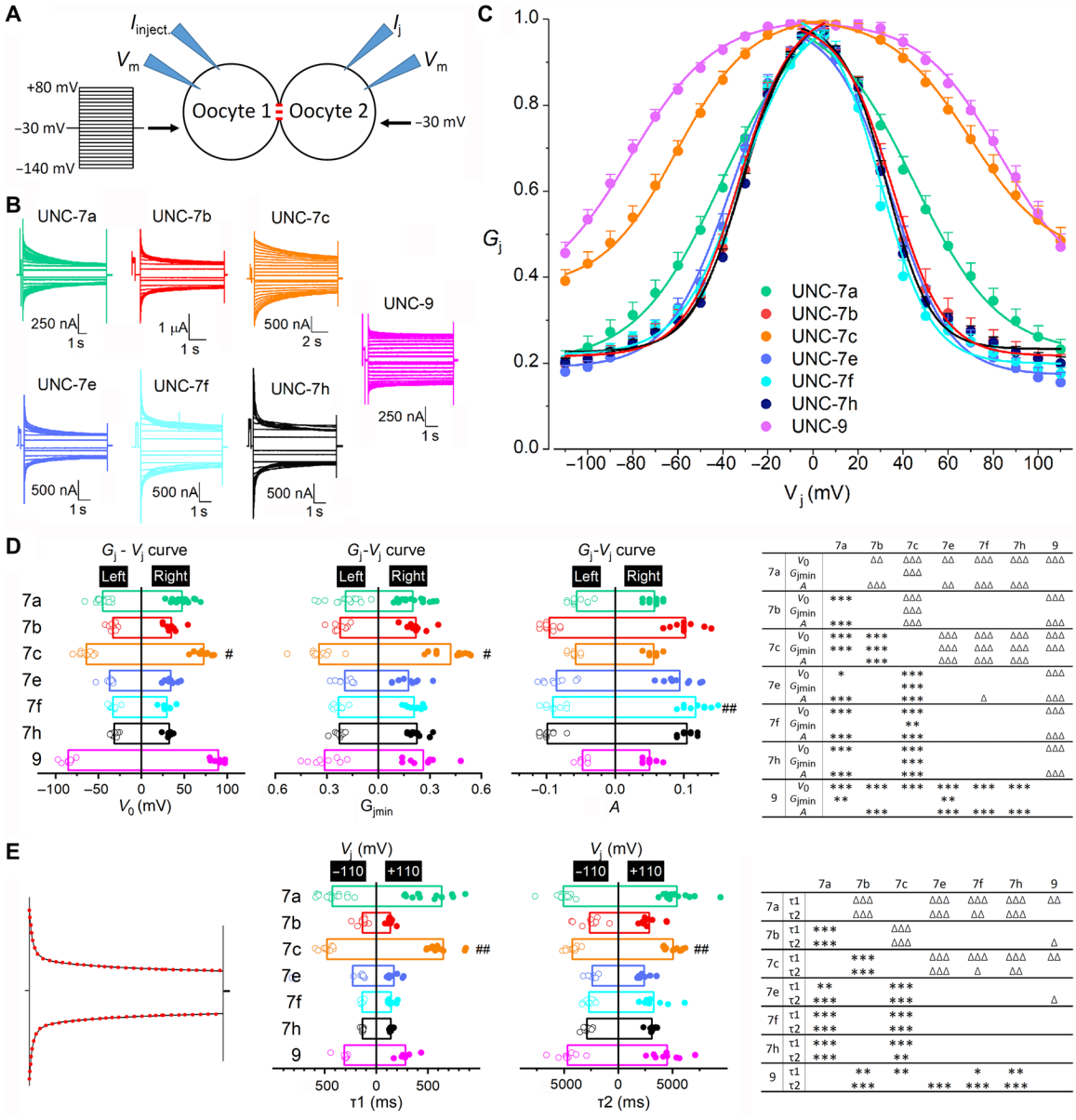

Fig. 2. Biophysical properties of UNC-7 and UNC-9 homotypic GJs expressed in *Xenopus* oocytes. (**A**) Diagram showing the oocyte experiment. (**B**) Representative I_j traces. (**C**) Normalized G_j-V_j relationships. (**D**) Comparisons of V_0, G_{jmin}, and A. (**E**) Comparisons of deactivation time constants of I_j traces at V_j −110 and +110 mV, which were fitted to a two-term exponential model (red dotted lines). In (D) and (E), significant differences between the left and right G_j-V_j curves are indicated by pound signs (#) (paired *t* test), whereas those between different GJs by asterisks (*) and triangles (Δ) for the left and right G_j-V_j curves, respectively (two-way mixed ANOVA with Tukey's post hoc test). $P < 0.05$, $P < 0.01$, and $P < 0.001$ are indicated by one, two, and three symbols, respectively. The number of oocyte pairs recorded (*n*) was 16 UNC-7a, 10 UNC-7b, 12 UNC-7c, 9 UNC-7e, 10 UNC-7f, 11 UNC-7h, and 9 UNC-9.

(Fig. 4C). The different effects of the *unc-7(e5)* mutation and the *unc-7b* knockout on electrical coupling are due to differences in *unc-7* molecular lesion. While UNC-7b was selectively eliminated in the *unc-7b* knockout strain, all the UNC-7 isoforms are absent in the *unc-7(e5)* mutant, which is a putative null resulting from a premature stop codon in the predicted first extracellular loop of UNC-7 (*19*). The deficiency of I_j between AVA and VA5 in the *unc-7(e5)* mutant was rescued substantially when wild-type UNC-7b was expressed specifically in AVA using a Cre-LoxP approach (Fig. 4D). To determine whether the rescuing effect depends on a specific UNC-7 isoform, we tested the effect of AVA-targeted expression of UNC-7a in AVA of *unc-7(e5)* using the same approach. UNC-7a was chosen because an earlier study showed that its putative expression in a small number of neurons including AVA can rescue a locomotion defect of the *unc-7* mutant (*16*). Unexpectedly, although UNC-7a could form functional heterotypic GJs with UNC-9 in the *Xenopus* oocyte expression system, it did not cause any appreciable improvement in the AVA/A-MN coupling in the *unc-7(e5)* mutant (Fig. 4D). We therefore asked whether UNC-7a could be properly expressed in AVA by tagging it with GFP. We found that, while UNC-7a::GFP resembled UNC-7a in forming both homotypic and heterotypic GJs (with UNC-9) in the *Xenopus* oocyte expression

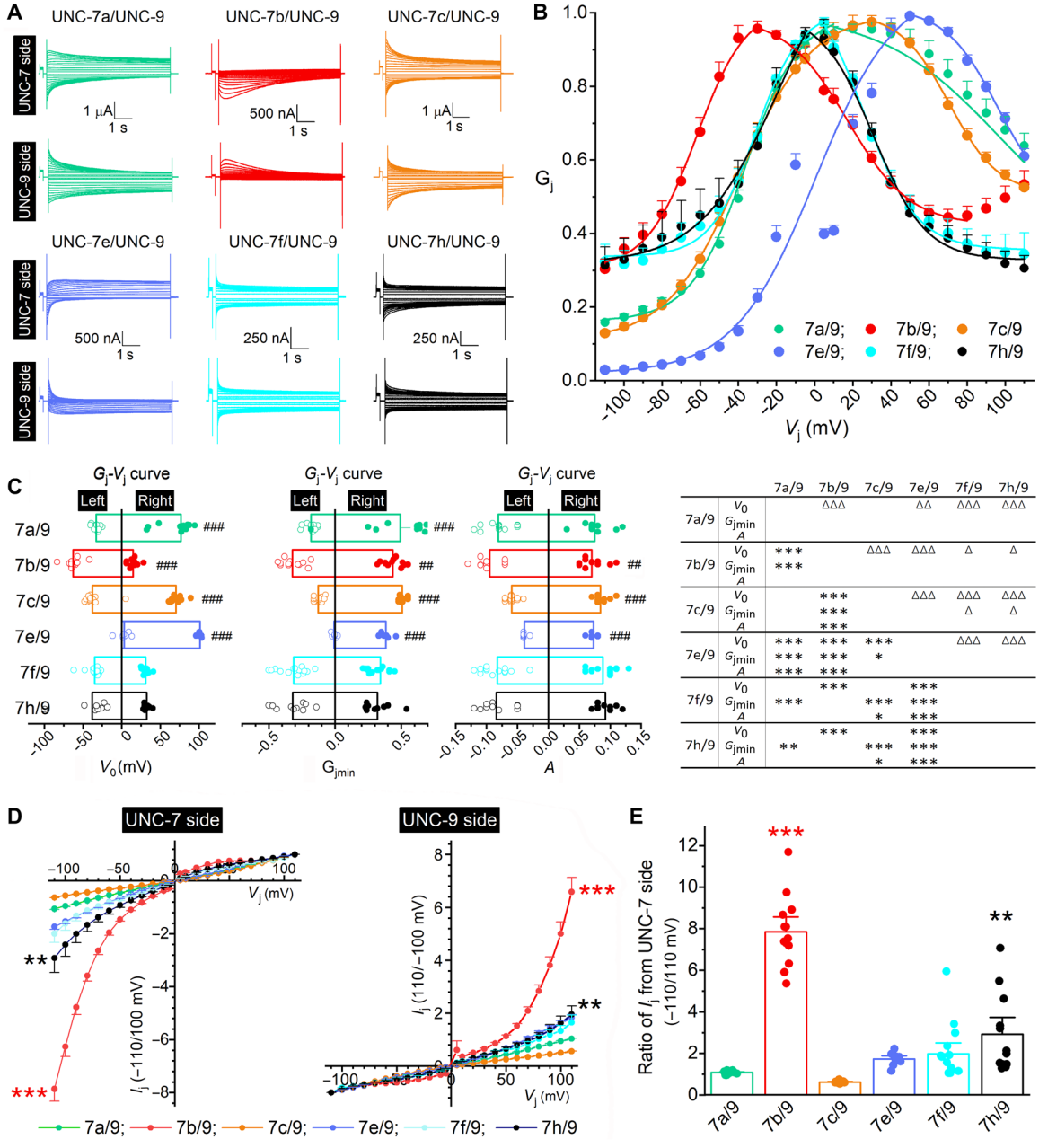

		7a/9	7b/9	7c/9	7e/9	7f/9	7h/9
7a/9	V_0		ΔΔΔ		ΔΔ	ΔΔΔ	ΔΔΔ
	G_{jmin}						
	A						
7b/9	V_0	***		ΔΔΔ	ΔΔΔ	Δ	Δ
	G_{jmin}	***					
	A						
7c/9	V_0		***		ΔΔΔ	ΔΔΔ	ΔΔΔ
	G_{jmin}		***			Δ	Δ
	A		***				
7e/9	V_0	***	***	***		ΔΔΔ	ΔΔΔ
	G_{jmin}	***	***	*			
	A	***	***				
7f/9	V_0		***		***		
	G_{jmin}	***		***	***		
	A			*	***		
7h/9	V_0		***		***		
	G_{jmin}	**		***	***		
	A			*	***		

Fig. 3. Biophysical properties of UNC-7 and UNC-9 heterotypic GJs expressed in *Xenopus* oocytes. (**A**) Representative I_j traces. (**B**) Normalized G_j-V_j relationships based on I_j recorded from the UNC-7 oocyte. (**C**) Comparisons of V_0, G_{jmin}, and A. Significant differences between the left and right G_j-V_j curves are indicated by pound signs (#) (paired t test), whereas those between different GJs by asterisks (*) and triangles (Δ) for the left and right G_j-V_j curves, respectively (two-way mixed ANOVA with Tukey's post hoc test). (**D**) Comparison of peak I_j-V_j curves between different GJs. Peak I_j were normalized by that of the same recording at either +110 or −110 mV V_j. (**E**) Comparisons of peak I_j ratios (−110 over 110 mV) for I_j recorded from the UNC-7 oocyte. In (D) and (E), significant differences from the nonrectifying UNC-7a/UNC-9 GJs are indicated by asterisks (*P < 0.01 and ***P < 0.001) based on two-way mixed (D) or one-way (E) ANOVA with Tukey's post hoc test. The number of oocyte pairs recorded (n) was 12 UNC-7a/UNC-9, 13 UNC-7b/UNC-9, 14 UNC-7c/UNC-9, 9 UNC-7e/UNC-9, 15 UNC-7f/UNC-9, and 12 UNC-7h/UNC-9.

system (fig. S4A), no GFP signal could be detected in AVA after the fusion protein was expressed using the Cre-LoxP approach (fig. S4B). The failure to detect UNC-7a::GFP expression in AVA likely accounts for the failure of UNC-7a in rescuing the AVA/A-MN coupling defect of *unc-7(e5)* mutant. Together, our results suggest that UNC-7b in AVA is important to the AVA/A-MN coupling.

Rectification depends on charged residues in the UNC-7b N terminus

Why is UNC-7b unique in being able to form strongly rectifying GJs with UNC-9? To answer this question, we explored potential roles of some charged amino acid residues in the UNC-7b N terminus. Two triplets of oppositely charged amino acid residues (HKK

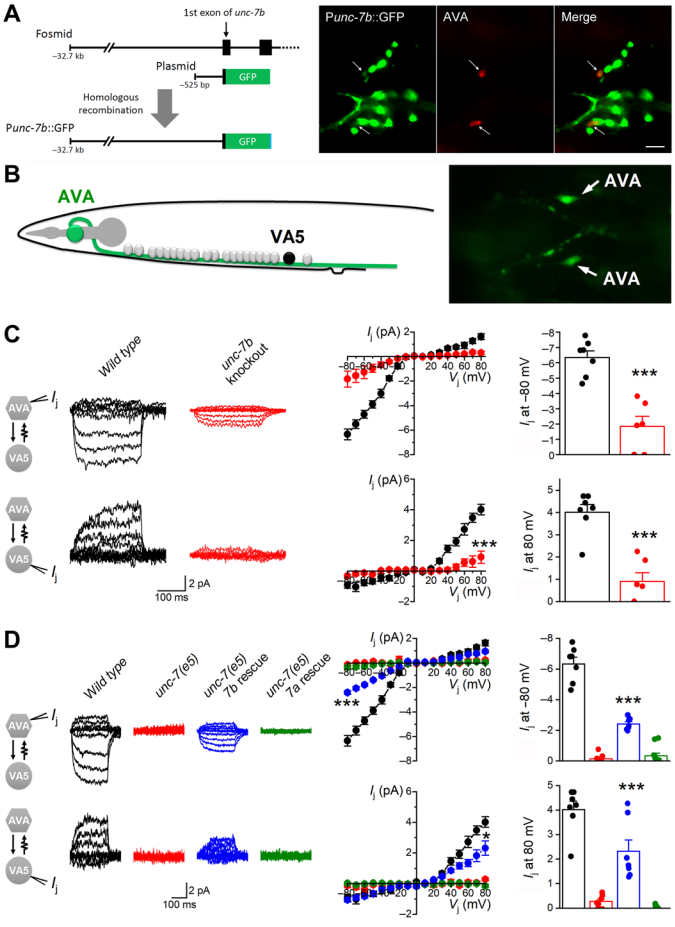

Fig. 4. UNC-7b is expressed in AVA and is important to AVA/A-MN coupling. (**A**) *unc-7b* expression in AVA. Left: Diagram showing the use of an in vivo homologous recombination approach to generate a P*unc-7b*::GFP transcriptional fusion. A plasmid containing 525 bp of the proximal *unc-7b* promoter (P*unc-7b*) and a portion of the *unc-7b* first exon fused in-frame to GFP was coinjected with the fosmid WRM0613cD09, which contains the entire *unc-7* gene, into an existing strain with AVA labeled by mStrawberry. Right: GFP expression was observed in the two AVA interneurons labeled by mStrawberry. (**B**) A diagram and an image showing the identification of VA5 and AVA based on anatomic location and GFP labeling, respectively, in electrophysiological recordings. (**C**) Knockout of *unc-7b* eliminated most I_j between AVA and VA5. (**D**) AVA-specific expression of wild-type UNC-7b but not UNC-7a significantly rescued the coupling defect of the null mutant *unc-7(e5)*. Data in (C) and (D) were statistically analyzed together (two-way mixed ANOVA). Statistically significant differences compared with wild type (C) or *unc-7(e5)* (D) are indicated (* $P < 0.05$, *** $P < 0.001$). The number of worms analyzed (*n*) was 7 wild type, 6 *unc-7b* knockout, 7 *unc-7(e5)*, 7 *unc-7(e5)* with AVA-specific UNC-7b rescue, and 11 *unc-7(e5)* with AVA-specific UNC-7a rescue.

and DDD) in the UNC-7 N terminus caught our attention (Fig. 5A). Although these two triplets of charged residues are not unique to UNC-7b (Fig. 1C), electrostatic interactions between them might stabilize a conformation that allows the unique N terminus of UNC-7b (the ball) to bind to a receptor site to block the GJ pore (Fig. 5B). To test this hypothesis, we neutralized the two triplets of charged residues in UNC-7b ($H^{45}K^{46}K^{47}$ and $D^{70}D^{71}D^{72}$) independently by alanine substitution and examined the effects of the mutations on the biophysical properties of UNC-7b/UNC-9 GJs using the *Xenopus* oocyte expression system. The rectification property was abolished by the DDD to AAA mutation and greatly compromised by the HKK to AAA mutation (Fig. 5, C and D). We suspected that the incomplete inhibitory effect of the HKK to AAA mutation might be due to other molecular structural differences between the original residues and the alanine residues. Among the noncharged amino acid residues, phenylalanine (F) and glutamine (Q) are most similar to H and K, respectively, in structure. We found that replacing the HKK residues in UNC-7b by FQQ essentially abolished the rectification property of UNC-7b/UNC-9 GJs (Fig. 5, C and D).

We next tested whether UNC-7b can still confer the rectification property to heterotypic GJs with UNC-9 after switching the locations of the two triplets of charged residues (HKK and DDD). We found that the mutated UNC-7b (DDD/KKH) did not retain the ability of conferring rectification (Fig. 5, E and F). We wondered whether a combination of switching the locations of DDD and HKK and replacing them with other similarly charged residues may allow UNC-7b to regain its rectification capability by testing the effects of EEE/KKK and DDD/KKK mutations. However, these two mutated UNC-7b isoforms also did not allow UNC-7b to regain its ability of conferring rectification (Fig. 5, E and F). These results suggest that the locations of the two triplets of charged residues are also important to the proper function of UNC-7b.

Last, we examined the effect of neutralizing two lysine residues ($K^{13}K^{14}$) in the unique N terminus of UNC-7b. We found that the mutation led to reduced peak I_j recorded from the UNC-9 but not from the UNC-7b oocyte in UNC-7b/UNC-9 heterotypic GJs (Fig. 5, C and D). Because the peak I_j recorded from the UNC-7b and UNC-9 oocytes had identical driving force but resulted from depolarizing the UNC-9 oocyte and hyperpolarizing the UNC-7b oocyte, respectively, the results suggest that the presence of these two lysine residues may modulate GJ gating in a membrane voltage–dependent manner. Presumably, the two lysine residues may enhance conductance of the heterotypic GJ due to an electrostatic force from the negative electric field of UNC-7b oocyte hyperpolarization (Fig. 5B).

DISCUSSION

This study shows that UNC-7b is a key component of the rectifying GJs between AVA and A-MNs in *C. elegans* escape neural circuit and that its N terminus plays a critical role in the rectification. These conclusions are supported by multiple lines of evidence, including strongly rectified peak and steady-state I_j of UNC-7b/UNC-9 GJs in the *Xenopus* oocyte expression system, correspondence of I_j rectification direction between the oocyte expression system and AVA/A-MN coupling, rescue of *unc-7* mutant coupling defect by AVA-specific expression of UNC-7b, deficiency of AVA/A-MNs coupling in *unc-7b* knockout strain, and loss of the rectification property after neutralizing either one of two clusters of oppositely charged residues in UNC-7b N terminus. Given that GJs are observed throughout *C. elegans* nervous system (*20*) and that both UNC-7 and UNC-9 are expressed in many neurons (*21*, *22*), it is conceivable that UNC-7b might also confer rectification properties to GJs elsewhere to affect circuit dynamics and behaviors.

Our analyses of mutating charged amino acid residues in UNC-7b N terminus favor a model in which the rectification property of UNC-7b/UNC-9 GJs depends on a ball-and-receptor mechanism (Fig. 6). However, this model appears to be in conflict with the facts that homotypic UNC-7b GJs were conductive and that the HKK

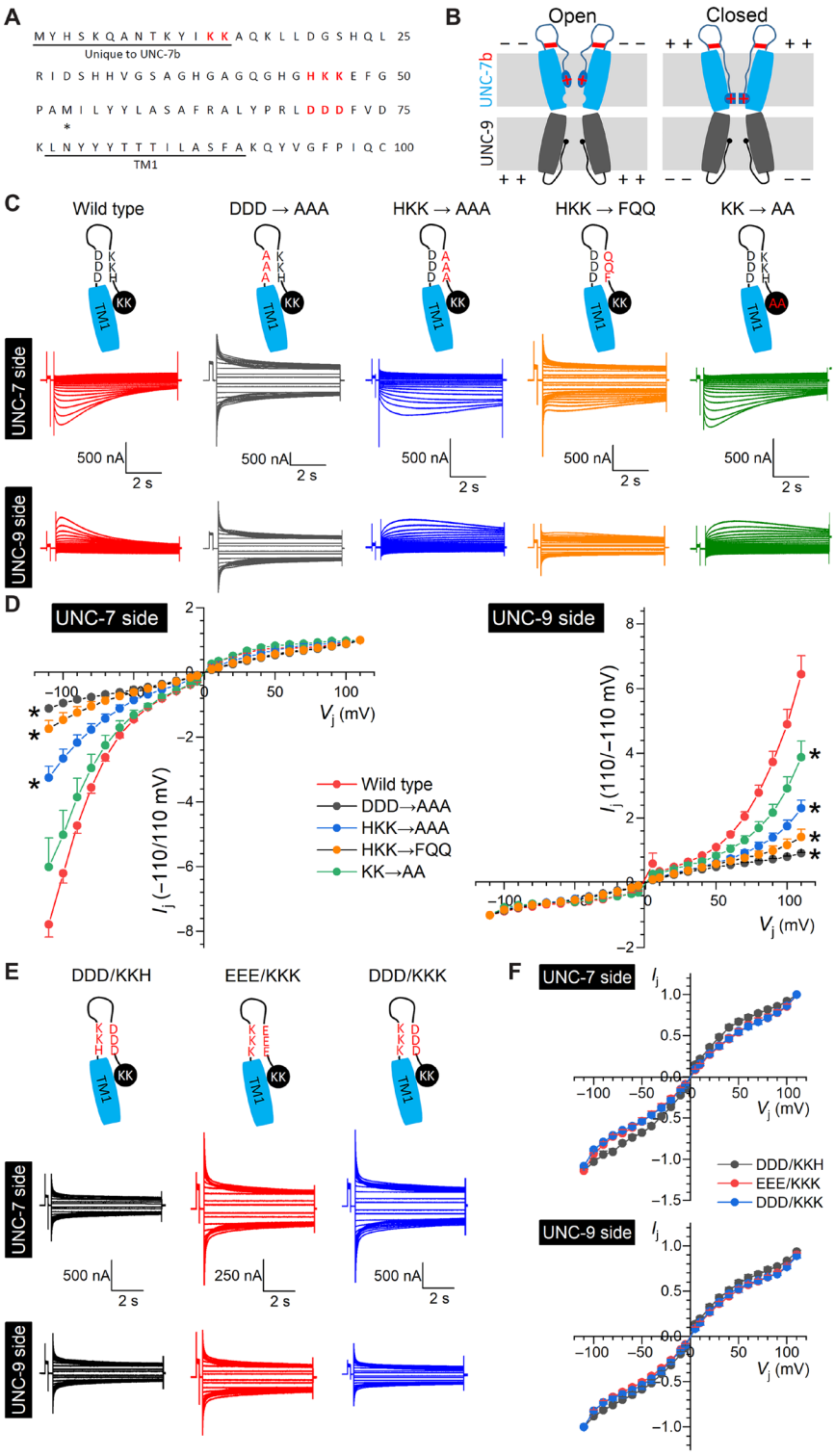

Fig. 5. Rectification of UNC-7b/UNC-9 heterotypic GJs depends on charged residues in UNC-7b N terminus. (**A**) Amino acid sequence of UNC-7b N terminus. (**B**) Model of UNC-7b/UNC-9 GJ gating. UNC-7b N terminus (the ball) may bind to a putative receptor site in a V_j-dependent manner to gate the GJ. The red lines represent electrostatic interactions between the two triplets of oppositely charged residues ["HKK" and "DDD" residues in (A)], whereas the plus sign (+) represents the $K^{13}K^{14}$ residues in UNC-7b. (**C**) Representative I_j traces showing the effects of neutralizing charged residues in UNC-7b. (**D**) Normalized I_j-V_j relationships of peak I_j. The asterisk (*) indicates $P < 0.001$ compared with wild type (the same data in Fig. 3D, two-way mixed ANOVA). Pairs of oocytes recorded (from UNC-7b/UNC-9 oocytes) were 10/9 DDD ➔ AAA, 13/11 HKK ➔ AAA, 11/10 HKK ➔ FQQ, and 11/9 KK ➔ AA. (**E**) Representative I_j traces showing the effects of swapping the locations of the two triplets of oppositely charged amino acid residues. (**F**) Peak I_j-V_j relationships. Peak I_j were normalized by that of each recording at either +110 or −110 mV. Pairs of oocytes recorded were 5 to 10 per group.

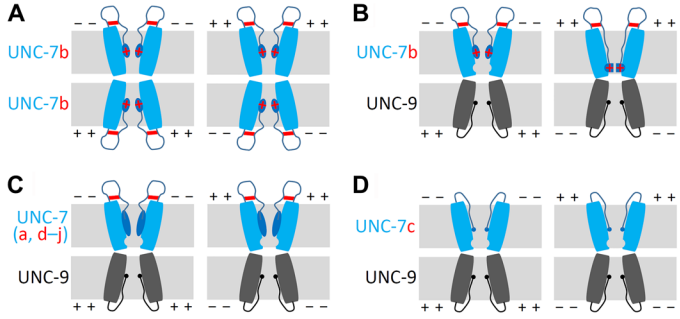

Fig. 6. A ball and receptor model of UNC-7/UNC-9 heterotypic GJ gating. (**A**) Homotypic UNC-7b GJs are conductive because of the absence of a receptor side for the N terminus ball. (**B**) A receptor site for the ball (represented by an indentation facing the channel pore) is induced in the UNC-7 hemichannel by UNC-9 hemichannel docking. Interactions between the ball and the receptor depend on putative salt bridges between HKK and DDD (represented by horizontal red lines) and V_j polarity. The ball binds to the receptor site to block the channel pore when UNC-7b cell is more depolarized than UNC-9 cell but detach from the receptor site when UNC-9 cell is more depolarized than UNC-7b cell. The K^{13} and K^{14} charged residues in UNC-7b's unique N terminus sequence (represented by red crosses) impact GJ gating in a membrane voltage-dependent manner. Specifically, a more hyperpolarized membrane potential of UNC-7b cell enhances GJ conductance due to a stronger pulling effect on the N-terminal ball from a negative electric field produced by hyperpolarization of the UNC-7b cell. (**C**) The N termini of the other UNC-7 isoforms (except for UNC-7c) are too big to fit in the receptor site. (**D**) UNC-7c does not confer rectification because it lacks the necessary residues to form the HKK-DDD salt bridges. The solid blue and black spheres represent the N termini of UNC-7c and UNC-9, respectively. The plus and minus symbols indicate whether the membrane potential of one cell is more depolarized or hyperpolarized compared with that of the contacting cell.

and DDD resides are not unique to UNC-7b. These two apparent conflicts could be reconciled by introducing the elements of an UNC-9–inducible receptor site in UNC-7b innexon and a size constraint of the N terminus ball to fit within the putative receptor site. In this model, docking of UNC-9 innexon with UNC-7b innexon induces a putative receptor site for UNC-7b N terminus. UNC-7b homotypic GJs are conductive due to the absence of the receptor site. UNC-7c N terminus cannot plug the GJ because it lacks the HKK residues. Although the other UNC-7 isoforms also have the two triplets of charged residues, their N-terminal balls are too big to fit into the receptor site. Our model also explains why UNC-7f and UNC-7h, which have slightly longer N terminus lengths than UNC-7b, could occasionally cause strong I_j rectification, and why the two positively charged residues (K^{13} and K^{14}) in UNC-7b may promote V_j-dependent gating. Although we cannot exclude other possibilities, this model appears to be the most plausible one for explaining how UNC-7 and UNC-9 may form the strongly rectifying heterotypic GJs between AVA and A-MNs.

Both *unc-7* and *unc-9* mutants show irregular body bends and greatly reduced forward locomotion activity compared with wild type (*16*, *23*). Previous studies have determined that two pairs of premotor interneurons, AVB and AVA, play central roles in locomotion. While AVA is important to backward locomotion and contacts cholinergic A-MNs through both chemical synapses and ESs, AVB is important to forward locomotion and contacts B-type cholinergic MNs (B-MNs) through ESs only (*24*). An earlier study identified the first three isoforms of UNC-7, including UNC-7a (UNC-7 L), UNC-7b (UNC-7S), and UNC-7c (UNC-7SR), and suggested that the GJs between AVB and B-MNs consist of UNC-7b in AVB and UNC-9 in B-MNs (*19*). However, biophysical properties of the GJs between AVB and B-MNs and the putative role of UNC-7b in the coupling have not been examined by electrophysiological analyses. A subsequent study showed that expressing wild-type UNC-7a under the control of either *nmr-1* or *rig-3* promoter may rescue locomotion defect of an *unc-7* mutant (*16*). Because both promoters are active in AVA but not AVB, the results suggest that UNC-7a may function in AVA to establish the AVA/A-MN coupling. However, we found that UNC-7a had no rescuing effect on the AVA/A-MN coupling in *unc-7* mutant worms, possibly due to a failure of UNC-7a expression in AVA. In agreement with our observation, an earlier study detected neither a rescuing effect of wild-type UNC-7a on *unc-7* mutant behavior nor the expression of UNC-7a::GFP fusion protein in transgenic worms (*19*). We speculate that the rescuing effect of UNC-7a on locomotion defects of an *unc-7* mutant in the previous study (*16*) could be due to UNC-7a function in other neurons because the *nmr-1* and *rig-3* promoters used for AVA-targeted expression also have activities in some other neurons (www.wormbase.org).

Two obvious questions arose from this study. Why did a small amount of I_j persist in the *unc-7b* knockout strain? Why could not the AVA/A-MN coupling defect of an *unc-7* mutant be fully rescued by expressing UNC-7b specifically in AVA? One possibility is that the UNC-7 innexon in AVA is a heteromeric complex consisting of UNC-7b and another UNC-7 isoform, and the presence of either alone is insufficient to form fully functional GJs with UNC-9. It is potentially a major challenge to identify the other putative UNC-7 isoform functioning in AVA given the large number of UNC-7 isoforms and the many conceivable experiments needed to properly address each one's possibility. Nevertheless, there is little doubt that UNC-7b is a key component of the GJs between AVA and A-MNs.

The I_j kinetics of UNC-7b/UNC-9 heterotypic GJs differed greatly from that of the UNC-7/UNC-9 GJs in vivo. Differences in regulatory proteins and posttranslational modifications between these two systems could potentially alter GJ functional properties. For example, UNC-9 GJs require UNC-1, a stomatin-like protein, to function in *C. elegans* (*25*, *26*) but not in *Xenopus* oocytes. The apparent dispensability of UNC-1 for UNC-9 GJs in *Xenopus* oocytes could be due to substitution of UNC-1 by an endogenous stomatin-like protein because the *Xenopus laevis* genome contains several stomatin-like genes (*27*). It is worth noting that the *Xenopus* oocyte expression system has been used to analyze biophysical properties of homotypic and heterotypic GJs formed by UNC-9 and two different isoforms of UNC-7 (a and b) (*19*). However, the earlier study did not detect any significant difference in biophysical properties between UNC-7a and UNC-7b homotypic GJs and between UNC-7a/UNC-9 and UNC-7b/UNC-9 heterotypic GJs. It was concluded that the N terminus of UNC-7 has little effect on voltage gating of GJs. It is unclear why the previous study failed to detect the effects of UNC-7 N terminus on GJ function.

Although connexins and innexins belong to two different families of proteins, GJs formed by them share major structural and functional properties. For example, N termini of both connexins and innexins are positioned at GJ permeation pathway space (*28*–*31*). Studies with connexins have led to the conclusions that N termini control V_j dependence (*15*, *32*–*35*), and this function depends on charged amino acid residues (*32*–*34*, *36*). The roles of UNC-7b N terminus in GJ gating reported here are in agreement with these structural and functional data of GJs. Thus, N termini might play an

evolutionarily conserved role in conferring rectification properties to neuronal GJs to affect neural circuit dynamics.

MATERIALS AND METHODS

C. elegans culture and strains

C. elegans hermaphrodites were grown on standard nematode growth medium plates with a layer of OP50 *Escherichia coli* at 22°C inside an environmental chamber. The following strains were used in this study (plasmids for making the transgenic strains are indicated by numbers with a "*wp*" prefix): ZW704: *zwEx175[Pflp-18::loxP::LacZ::STOP::loxP::mCherry::SL2::GFP(wp1383), Pgpa-14::Cre(pNP259)]*. ZW731: *zwEx175[Pflp-18::loxP::LacZ::STOP::loxP::mCherry::SL2::GFP(wp1383), Pgpa-14::Cre(pNP259)]; unc-7(e5)*. ZW1121: *zwEx175[Pflp-18::loxP::LacZ::STOP::loxP::mCherry::SL2::GFP(wp1383), Pgpa-14::Cre(pNP259)]; unc-7(zw98)*. ZW1251: *zwEx175[Pflp-18::loxP::LacZ::STOP::loxP::mCherry::SL2::GFP(wp1383), Pflp-18::loxP::LacZ::STOP::loxP::unc-7a(wp1677), Pgpa-14::Cre(pNP259)]; unc-7(e5)*. ZW1252: *zwEx175[Pflp-18::loxP::LacZ::STOP::loxP::mCherry::SL2::GFP(wp1383), Pflp-18::loxP::LacZ::STOP::loxP::unc-7b(wp1678), Pgpa-14::Cre(pNP259)]; unc-7(e5)*. ZW1414: *zwIs143[Pflp-18::loxP::LacZ::STOP::loxP::mStrawberry(wp1392), Pgpa-14::Cre(pNP259), lin-15(+)]; zwEx261 [Punc-7b::GFP (wp1691 + p1692)]*. ZW1531: *zwEx276[Pflp-18::loxP::LacZ::STOP::loxP::UNC-7a::EGFP(wp1961), Pflp-18::loxP::LacZ::STOP::loxP::mStrawberry(wp1339), Pgpa-14::Cre(pNP259)]; unc-7(e5)*.

cDNA cloning

unc-7a complementary DNA (cDNA) was cloned by nested reverse transcription polymerase chain reaction (RT-PCR) using a first-strand cDNA library of wild-type worms as the template. The sense/antisense primers used for the first and second PCRs were 169/170 and 171/664, respectively. The second PCR product was cloned into the oocyte expression vector pXMX-T3(−) at BamH1/EcoR1 sites to produce the *unc-7a* plasmid (*wp776*). *unc-7b* cDNA was obtained by PCR using plasmid *wp776* as the template and the 2036/3036 sense/antisense primer pair. Primer 2036 contained 5′-end sequence unique to *unc-7b* cDNA, while primer 3036 is complementary to the common 3′-end of *unc-7* cDNAs. The PCR product was cloned into pXMX-T3(−) at Xho1/Age1 sites to produce the *unc-7b* plasmid (*wp1275*). *unc-7c* cDNA was cloned by PCR using *wp776* as the template and the 1854/3036 sense/antisense primer pair. The PCR product was cloned into pXMX-T3(−) at BamH1/Age1 sites to produce the *unc-7c* expression plasmid (*wp1239*). *unc-7e* cDNA was cloned by nested RT-PCR using a first-strand cDNA library of wild-type worms as the template. The sense/antisense primers used for the first and second PCRs were 3491/3492 and 3539/3540, respectively. The second PCR product was cloned into pXMXT-3(−) at Pst1/Age1 sites to produce the *unc-7e* expression plasmid (*wp1742*). *unc-7f* cDNA was cloned by PCR using plasmid *wp776* as the template and the 3695/3036 sense/antisense primer pair. Primer 3695 contained 5′-end sequence unique to *unc-7 f*. The PCR product was cloned into pXMX-T3(−) at BamH1/Age1 sites to produce the *unc-7f* plasmid (*wp1814*). *unc-7h* cDNA was cloned by two steps of PCR using plasmid *wp776* as the template. The sense/antisense primers used for the first and second steps were 3696/3036 and 3697/3036, respectively. The sense primers 3696 and 3697 contained 5′-end sequence unique to *unc-7 h*. The second PCR product was cloned into pXMX-T3(−) at BamH1/Age1 sites to produce the *unc-7h* plasmid (*wp1815*). The *unc-9* plasmid (*wp778*) was produced by cutting out an *unc-9* cDNA insert from a previously described plasmid (*37*) and cloning it into pXMX-T3(−) at BamH1/Age1 sites. Sequences of the primers used for cloning *unc-7* cDNAs are listed in table S5. The *unc-7a*::GFP plasmid for oocyte expression (*wp1960*) was made through two sequential steps: (i) clone enhanced GFP (EGFP) coding sequence from an existing plasmid (*wp757*) into another plasmid (*wp572*) at Age1 and Nhe1 sites to make *wp1959*, in which EGFP coding sequence was fused in-frame to the 3′-end of *unc-7a*, and (ii) clone the *unc-7a::egfp* insert from *wp1959* into *wp776* at BamH1 and EcoR1 sites (to replace the *unc-7a* insert).

cRNA expression

The *unc-7* and *unc-9* plasmids described above were linearized using the restriction enzyme Fsp I and used as templates for synthesizing cRNAs. Capped cRNAs were synthesized using a mMESSAGE mMACHINE T3 Transcription kit (AM1348, Thermo Fisher Scientific). Each cRNA injection solution was a mixture of a specific cRNA (500 to 800 ng/μl) and two connexin 38 antisense oligonucleotides (100 ng/μl each). Nucleotide sequences of the two oligonucleotides were 5′-GCTTTAGTAATTCCCATCCTGCCATGTTTC-3′ and 5′-AGCAGAAGAGTATACTTCTGTTTGT-3′ (*38*). Approximately 50 nl of the mixture was injected per oocyte using a Drummond Nanoject II injector (Drummond Scientific). The vitelline membrane of the oocyte was removed using a pair of #5 Dumont Tweezers (500341, Word Precision Instruments, Sarasota, FL) during the pairing process. Oocyte pairing and subsequent recordings were performed in a 3-ml petri dish, in which a small cutout piece of Nunc MicroWell MiniTray (438733, Nalge Nunc International, Rochester, NY) was glued to the bottom with two oocytes placed inside each well, as described by others (*38*). Injected oocytes were incubated in ND96 solution [96 mM NaCl, 2 mM KCl, 1.8 mM $CaCl_2$, 1 mM $MgCl_2$, and 5 mM Hepes (pH 7.5)] for 2 to 5 days inside an environmental chamber (15°C) before being paired. Paired oocytes were incubated in ND96 solution for 12 to 24 hours at the room temperature (20° to 22°C) before electrophysiological recordings.

Oocyte electrophysiology

Voltage-clamp recordings were performed using two Oocyte Clamp amplifiers (OC-725C, Warner Instruments LLC, Hamden, CT) equipped with differential voltage probes (7255DI, Warner Instruments). The amplifiers were set to high side current measuring mode to record I_j. Current and voltage electrodes (resistance, 1.5 to 1.8 megohm) as well as differential voltage electrodes were pulled from borosilicate glass capillaries (TW150F-4, World Precision Instruments). Tips of the differential voltage electrodes were manually broken to a larger size (resistance, ~0.2 megohm), filled with ND96 solution, and connected to the headstages via microelectrode holders (MEH1S15, World Precision Instruments). The two oocytes of each pair were held at −30 mV, from which a series of voltage steps (−150 to +90 mV) were applied to one oocyte, while the other was held constant at −30 mV to record I_j. Subsequently, the voltage protocol was repeated but with the two oocytes swapped in being the receiver of voltage steps and the monitor of I_j. The intervals between consecutive V_j steps were 10 mV except for the additions of −5 and +5 mV steps. In each recording, positive and negative V_j steps were applied alternatively from high to low (e.g., +120, −120, +110, −110, ……, +10, −10, +5, −5 mV). I_j from the first two V_j steps (+120 and −120 mV) were excluded in subsequent data analyses. Data were filtered at

1000 Hz and sampled at 2000 Hz. The use of frogs followed the Institutional Animal Care and Use Committee guidelines and was approved by the Institutional Review Board.

unc-7b knockout

unc-7b isoform–specific knockout was achieved using a CRIPR-Cas9 approach. Specifically, a 19-bp guiding sequence identical to the target sequence in the first exon of *unc-7b* was cloned into a pDD162 vector (P*eft-3*::*Cas9* + empty single guide RNA, Addgene #47549). The resultant construct was coinjected with a repairing primer (3475), in which a stop codon was introduced. Knockout worms were identified by PCR using a pair of specific primers (3476/3477) and confirmed by sequencing.

unc-7 mutant rescue

cDNAs encoding wild-type UNC-7b, wild-type UNC-7a, and UNC-7a::GFP were expressed in AVA interneurons of *unc-7(e5)* using two promoters (P*flp-18* and P*gpa-14*) in a Cre-LoxP approach (*39*). In these experiments, *unc-7a* and *unc-7b* cDNAs were cloned independently into *wp1338* (pCoS10, P*flp-18*::loxP::LacZ::STOP::loxP::ChR2::mCherry::SL2::GFP) (*39*) to generate two plasmids: *wp1677* (P*flp-18*(3.3 kb)::loxP::LacZ::STOP::loxP::UNC-7a) and *wp1678* (P*flp-18*(3.3 kb)::loxP::LacZ::STOP::loxP::UNC-7b). *wp1961* (P*flp-18*(3.3 kb)::loxP::LacZ::STOP::loxP::UNC-7a::GFP) was made by cloning *unc-7a::egfp* insert from *wp1959* into *wp1677* at Nhe1 and Nco1 sites. The three plasmids (*wp1677*, *wp1678*, and *wp1961*) were independently coinjected with *wp1339* (pNP259: P*gpa-14*::Cre) into *unc-7(e5)* mutant to achieve AVA-targeted expression (*39*). AVA interneurons in these transgenic strains were labeled by GFP using the same approach.

Site-directed mutagenesis

Plasmids for expressing various mutated isoforms of UNC-7b in *Xenopus* oocytes were created by mutating *wp1275* using specific sense and antisense primer pairs and PfuUltra (Agilent Technologies, La Jolla, CA, USA) in a PCR-based approach (QuickChange Site-Directed Mutagenesis). The *unc-7b* cDNA insert region of each newly generated plasmid was fully sequenced to confirm that only the intended mutation had been introduced into *unc-7b*.

unc-7b expression pattern determination

A short genomic fragment (563 bp) encompassing part of the first exon of *unc-7b* and immediate upstream sequence was amplified by PCR using the primer pair 3382/3383 and fused to GFP in a worm expression vector derived from pPD118.20. The resultant plasmid (*wp1692*) was linearized with Hind III and coinjected into *lin-15(n765)* with the fosmid WRM0613cD09, which was linearized with Tth III and a *lin-15* rescue plasmid. To determine whether *unc-7b* is expressed in AVA interneurons, the transgene was crossed into an integrated strain expressing mStrawberry in AVA (*ZW1140*), which was created by coinjecting *wp1392* (P*flp-18*::loxP::LacZ::STOP::loxP::mStrawberry), *wp1339*, and a *lin-15* rescuing plasmid into *lin-15(n765)*.

C. elegans electrophysiology

All electrophysiological experiments were performed with adult hermaphrodites. An animal was immobilized by applying Vetbond Tissue Adhesive (3M Company, St. Paul, MN) to the dorsal anterior portion, allowing its tail to sway freely during the experiment. A longitudinal incision was made along the glued region to expose AVA and VA5. After clearing the viscera by suction through a glass pipette, the cuticle flap was folded back and glued to the coverslip. The dissected worm preparation was treated with collagenase A (0.5 mg $ml^{-1;}$ Roche Applied Science, catalog number 10103578001) for 10 to 15 s and perfused with the extracellular solution for 5- to 10-fold of bath volume. VA5 motor neuron was identified on the basis of its anatomical location, whereas identification of AVA was helped by expressing GFP in AVA using two promoters and the *Cre-LoxP* approach (*39*). Microelectrodes (resistance, ~20 megohm), pulled from borosilicate glass capillaries (BF120-69-10, Sutter Instruments, Novato, CA, USA) and fire polished, were used for dual-neuron voltage clamp recordings with an amplifier (MultiClamp 700B, Molecular Devices, Sunnyvale, CA, USA) and the Clampex software (version 10, Molecular Devices). Classical whole-cell configuration was obtained by applying a negative pressure to the recording pipette. I_j were recorded by holding either AVA or VA5 at −30 mV, while its counterpart was stepped to a series of membrane voltages (−110 to +50 mV). Data were filtered at 2 kHz and sampled at 10 kHz. The pipette solution contained 120 mM KCl, 20 mM KOH, 5 mM tris, 0.25 mM $CaCl_2$, 4 mM $MgCl_2$, 36 mM sucrose, 5 mM EGTA, and 4 mM Na_2ATP (pH 7.2). The bath solution contained 140 mM NaCl, 5 mM KCl, 5 mM CaCl2, 5 mM MgCl2, 11 mM dextrose, and 5 mM Hepes (pH 7.2).

Data analyses and graphing

Analyses of steady-state I_j of GJs in Xenopus oocytes

The averaged steady-state I_j from the last 500 ms of each V_j step were quantified and converted to G_j. Subsequently, the G_j of homotypic and heterotypic GJs were processed somewhat differently. For homotypic GJs, the G_j values over the negative and positive V_j ranges were first independently fitted to a Boltzmann function, $G_j = (1 - G_{jmin})/\{1 + \exp[A(V_j - V_0)]\} + G_{jmin}$, to extrapolate the G_{jmax} at 0 mV V_j, and then normalized on the basis of the extrapolated G_{jmax} to fit the Boltzmann function for a second time. The results from the second fit were used for statistical analyses. For heterotypic GJs, all the G_j values of each recording were normalized by the largest G_j (nominal G_{jmax}) from either the negative or positive V_j range. The ascending and descending portions of the resultant G_j-V_j relationship were independently fitted to the Boltzmann function with the fitting results used for statistical analyses. In the Boltzmann function, V_0 is the V_j at which G_j is half maximal, G_{jmin} is the minimum G_j, and A is a cooperativity constant. The dependable variables from the Boltzmann fit (V_0, G_{jmin}, and A) were compared between the positive and negative V_j ranges by paired t test and between the different GJs by one-way analysis of variance (ANOVA) followed by Tukey's tests using OriginPro 2019 (OriginLab, Northampton, MA, USA) and SPSS (IBM Corp., Armonk, NY, USA), respectively.

Analyses of peak I_j of heterotypic GJs in Xenopus oocyte

Peak I_j at each V_j step were quantified with ClampFit and normalized by the I_j at either −110 or +110 mV of V_j, as specified in figure legends, to plot the peak I_j-V_j relationship. In cases of strong rectification (e.g., all UNC-7b/UNC-9 GJs and several UNC-7f/UNC-9 and UNC-7h/UNC-9 GJs), the peak I_j on the small current side were quantified from the same time point of the peak I_j on the opposite side. The resultant peak I_j-V_j relationships and peak I_j ratios of the various heterotypic GJs were compared by either two-way mixed ANOVA or one-way ANOVA, as specified in figure legends. Statistically significant differences were detected with Tukey's tests.

Analyses of I_j between AVA and VA5

The averaged I_j between 100 and 200 ms of each V_j step were quantified with ClampFit and used to plot the I_j-V_j relationship, which was compared between different genotypes by a mixed ANOVA using SPSS with voltages as the within-subjects factor and genotypes as the between-subjects factor. Statistically significant differences were detected with Tukey's tests. Data are shown as means ± SE. $P < 0.05$ is considered as statistically significant. All graphs were made with Origin Pro.

SUPPLEMENTARY MATERIALS

Supplementary material for this article is available at http://advances.sciencemag.org/cgi/content/full/6/27/eabb3076/DC1

View/request a protocol for this paper from *Bio-protocol*.

REFERENCES AND NOTES

1. E. J. Furshpan, D. D. Potter, Transmission at the giant motor synapses of the crayfish. *J. Physiol.* **145**, 289–325 (1959).
2. J. E. Rash, S. Curti, K. G. Vanderpool, N. Kamasawa, S. Nannapaneni, N. Palacios-Prado, C. E. Flores, T. Yasumura, J. O'Brien, B. D. Lynn, F. F. Bukauskas, J. I. Nagy, A. E. Pereda, Molecular and functional asymmetry at a vertebrate electrical synapse. *Neuron* **79**, 957–969 (2013).
3. A. A. Auerbach, M. V. Bennett, A rectifying electrotonic synapse in the central nervous system of a vertebrate. *J. Gen. Physiol.* **53**, 211–237 (1969).
4. P. Phelan, L. A. Goulding, J. L. Y. Tam, M. J. Allen, R. J. Dawber, J. A. Davies, J. P. Bacon, Molecular mechanism of rectification at identified electrical synapses in the *Drosophila* giant fiber system. *Curr. Biol.* **18**, 1955–1960 (2008).
5. G. L. Ringham, Localization and electrical characteristics of a giant synapse in the spinal cord of the lamprey. *J. Physiol.* **251**, 395–407 (1975).
6. M. Wadepuhl, Depression of excitatory motoneurones by a single neurone in the leech central nervous system. *J. Exp. Biol.* **143**, 509–527 (1989).
7. L. Rela, L. Szczupak, Coactivation of motoneurons regulated by a network combining electrical and chemical synapses. *J. Neurosci.* **23**, 682–692 (2003).
8. S. Shruti, D. J. Schulz, K. M. Lett, E. Marder, Electrical coupling and innexin expression in the stomatogastric ganglion of the crab *Cancer borealis*. *J. Neurophysiol.* **112**, 2946–2958 (2014).
9. P. Liu, B. Chen, R. Mailler, Z.-W. Wang, Antidromic-rectifying gap junctions amplify chemical transmission at functionally mixed electrical-chemical synapses. *Nat. Commun.* **8**, 14818 (2017).
10. A. Devor, Y. Yarom, Electrotonic coupling in the inferior olivary nucleus revealed by simultaneous double patch recordings. *J. Neurophysiol.* **87**, 3048–3058 (2002).
11. G. J. Gutierrez, E. Marder, Rectifying electrical synapses can affect the influence of synaptic modulation on output pattern robustness. *J. Neurosci.* **33**, 13238–13248 (2013).
12. D. H. Edwards, S. R. Yeh, F. B. Krasne, Neuronal coincidence detection by voltage-sensitive electrical synapses. *Proc. Natl. Acad. Sci. U.S.A.* **95**, 7145–7150 (1998).
13. E. Marder, Electrical synapses: Beyond speed and synchrony to computation. *Curr. Biol.* **8**, R795–R797 (1998).
14. A. J. Marsh, J. C. Michel, A. P. Adke, E. L. Heckman, A. C. Miller, Asymmetry of an intracellular scaffold at vertebrate electrical synapses. *Curr. Biol.* **27**, 3561–3567.e4 (2017).
15. W. D. Marks, I. M. Skerrett, Role of amino terminus in voltage gating and junctional rectification of shaking B innexins. *J. Neurophysiol.* **111**, 1383–1395 (2014).
16. T. Kawano, M. D. Po, S. Gao, G. Leung, W. S. Ryu, M. Zhen, An imbalancing act: Gap junctions reduce the backward motor circuit activity to bias *C. elegans* for forward locomotion. *Neuron* **72**, 572–586 (2011).
17. A. Oshima, Structure of an innexin gap junction channel and cryo-EM sample preparation. *Microscopy* **66**, 371–379 (2017).
18. I. M. Skerrett, J. B. Williams, A structural and functional comparison of gap junction channels composed of connexins and innexins. *Dev. Neurobiol.* **77**, 522–547 (2017).
19. T. A. Starich, J. Xu, I. M. Skerrett, B. J. Nicholson, J. E. Shaw, Interactions between innexins UNC-7 and UNC-9 mediate electrical synapse specificity in the *Caenorhabditis elegans* locomotory nervous system. *Neural Dev.* **4**, 16 (2009).
20. J. G. White, E. Southgate, J. N. Thomson, S. Brenner, The structure of the nervous system of the nematode *Caenorhabditis elegans*. *Philos. Trans. R. Soc. Lond. B Biol. Sci.* **314**, 1–340 (1986).
21. A. Bhattacharya, U. Aghayeva, E. G. Berghoff, O. Hobert, Plasticity of the electrical connectome of *C. elegans*. *Cell* **176**, 1174–1189.e16 (2019).
22. Z. F. Altun, B. Chen, Z.-W. Wang, D. H. Hall, High resolution map of *Caenorhabditis elegans* gap junction proteins. *Dev. Dyn.* **238**, 1936–1950 (2009).
23. T. A. Starich, R. K. Herman, J. E. Shaw, Molecular and genetic analysis of *unc-7*, a *Caenorhabditis elegans* gene required for coordinated locomotion. *Genetics* **133**, 527–541 (1993).
24. M. de Bono, A. V. Maricq, Neuronal substrates of complex behaviors in *C. elegans*. *Annu. Rev. Neurosci.* **28**, 451–501 (2005).
25. B. Chen, Q. Liu, Q. Ge, J. Xie, Z.-W. Wang, UNC-1 regulates gap junctions important to locomotion in *C. elegans*. *Curr. Biol.* **17**, 1334–1339 (2007).
26. H. Jang, S. Levy, S. W. Flavell, F. Mende, R. Latham, M. Zimmer, C. I. Bargmann, Dissection of neuronal gap junction circuits that regulate social behavior in *Caenorhabditis elegans*. *Proc. Natl. Acad. Sci. U.S.A.* **114**, E1263–E1272 (2017).
27. A. M. Session, Y. Uno, T. Kwon, J. A. Chapman, A. Toyoda, S. Takahashi, A. Fukui, A. Hikosaka, A. Suzuki, M. Kondo, S. J. van Heeringen, I. Quigley, S. Heinz, H. Ogino, H. Ochi, U. Hellsten, J. B. Lyons, O. Simakov, N. Putnam, J. Stites, Y. Kuroki, T. Tanaka, T. Michiue, M. Watanabe, O. Bogdanovic, R. Lister, G. Georgiou, S. S. Paranjpe, I. van Kruijsbergen, S. Shu, J. Carlson, T. Kinoshita, Y. Ohta, S. Mawaribuchi, J. Jenkins, J. Grimwood, J. Schmutz, T. Mitros, S. V. Mozaffari, Y. Suzuki, Y. Haramoto, T. S. Yamamoto, C. Takagi, R. Heald, K. Miller, C. Haudenschild, J. Kitzman, T. Nakayama, Y. Izutsu, J. Robert, J. Fortriede, K. Burns, V. Lotay, K. Karimi, Y. Yasuoka, D. S. Dichmann, M. F. Flajnik, D. W. Houston, J. Shendure, L. DuPasquier, P. D. Vize, A. M. Zorn, M. Ito, E. M. Marcotte, J. B. Wallingford, Y. Ito, M. Asashima, N. Ueno, Y. Matsuda, G. J. C. Veenstra, A. Fujiyama, R. M. Harland, M. Taira, D. S. Rokhsar, Genome evolution in the allotetraploid frog *Xenopus laevis*. *Nature* **538**, 336–343 (2016).
28. S. Maeda, S. Nakagawa, M. Suga, E. Yamashita, A. Oshima, Y. Fujiyoshi, T. Tsukihara, Structure of the connexin 26 gap junction channel at 3.5 Å resolution. *Nature* **458**, 597–602 (2009).
29. A. Oshima, K. Tani, Y. Fujiyoshi, Atomic structure of the innexin-6 gap junction channel determined by cryo-EM. *Nat. Commun.* **7**, 13681 (2016).
30. P. E. Purnick, D. C. Benjamin, V. K. Verselis, T. A. Bargiello, T. L. Dowd, Structure of the amino terminus of a gap junction protein. *Arch. Biochem. Biophys.* **381**, 181–190 (2000).
31. J. B. Myers, B. G. Haddad, S. E. O'Neill, D. S. Chorev, C. C. Yoshioka, C. V. Robinson, D. M. Zuckerman, S. L. Reichow, Structure of native lens connexin 46/50 intercellular channels by cryo-EM. *Nature* **564**, 372–377 (2018).
32. S. Oh, S. Rivkin, Q. Tang, V. K. Verselis, T. A. Bargiello, Determinants of gating polarity of a connexin 32 hemichannel. *Biophys. J.* **87**, 912–928 (2004).
33. V. K. Verselis, C. S. Ginter, T. A. Bargiello, Opposite voltage gating polarities of two closely related connexins. *Nature* **368**, 348–351 (1994).
34. P. E. M. Purnick, S. Oh, C. K. Abrams, V. K. Verselis, T. A. Bargiello, Reversal of the gating polarity of gap junctions by negative charge substitutions in the N-terminus of connexin 32. *Biophys. J.* **79**, 2403–2415 (2000).
35. A. Oshima, K. Tani, M. M. Toloue, Y. Hiroaki, A. Smock, S. Inukai, A. Cone, B. J. Nicholson, G. E. Sosinsky, Y. Fujiyoshi, Asymmetric configurations and N-terminal rearrangements in connexin26 gap junction channels. *J. Mol. Biol.* **405**, 724–735 (2011).
36. H. Musa, E. Fenn, M. Crye, J. Gemel, E. C. Beyer, R. D. Veenstra, Amino terminal glutamate residues confer spermine sensitivity and affect voltage gating and channel conductance of rat connexin40 gap junctions. *J. Physiol.* **557**, 863–878 (2004).
37. Q. Liu, B. Chen, E. Gaier, J. Joshi, Z.-W. Wang, Low conductance gap junctions mediate specific electrical coupling in body-wall muscle cells of *Caenorhabditis elegans*. *J. Biol. Chem.* **281**, 7881–7889 (2006).
38. C. Peracchia, X. G. Wang, L. L. Peracchia, Chemical gating of gap junction channels. *Methods* **20**, 188–195 (2000).
39. C. Schmitt, C. Schultheis, S. J. Husson, J. F. Liewald, A. Gottschalk, Specific expression of channelrhodopsin-2 in single neurons of *Caenorhabditis elegans*. *PLOS ONE* **7**, e43164 (2012).

Acknowledgments: We thank C. Peracchia for help with the technique of recording junctional currents between *Xenopus* oocytes and K. Wang and K. Wacker for helpful comments about the manuscript. **Funding:** This study was supported by NIH R01NS109388 (to Z.-W.W.), NIH R01MN085927 (to Z-W.W.), and NIH GM113004 (to B.C.). **Author contributions:** Y.S. did all the *Xenopus* oocyte experiments, created the transgenic and knockout worm strains, and performed data analyses. P.L. did all the electrophysiological experiments with *C. elegans* and performed data analyses. H.Z. performed preliminary experiments. B.C. helped with experimental designs. Z.-W.W. oversaw the project and wrote the manuscript with inputs from co-authors. **Competing interests:** The authors declare that they have no competing interests. **Data and materials availability:** All data needed to evaluate the conclusions in the paper are present in the paper and/or the Supplementary Materials. Additional data related to this paper may be requested from the authors.

Submitted 14 February 2020
Accepted 20 May 2020
Published 3 July 2020
10.1126/sciadv.abb3076

Citation: Y. Shui, P. Liu, H. Zhan, B. Chen, Z.-W. Wang, Molecular basis of junctional current rectification at an electrical synapse. *Sci. Adv.* **6**, eabb3076 (2020).